This article has been accepted for inclusion in a future issue of this journal. Content is final as presented, with the exception of pagination.

High-Frequency Microwave Detection With GaN HEMTs in the Subthreshold Regime

Gaudencio Paz-Martínez, Ignacio Íñiguez-de-la-Torre, Philippe Artillan, Héctor Sánchez-Martín, Sergio García-Sánchez, Tomás González, *Senior Member, IEEE*, and Javier Mateos, *Member, IEEE*

***Abstract*— The behavior of GaN-based high-electron-mobility transistors (HEMTs) as microwave zero-bias detectors is very dependent on the configuration of the bias (current or voltage), the operation temperature, and whether the radio-frequency power is fed in the drain or the gate terminal. When the signal is injected into the drain, the negative current responsivity shows a bell-shape dependence on V_{GS} centered slightly above the threshold voltage for all the studied frequencies (1–43 GHz) and temperature ranges (8–400 K). In the case of the voltage responsivity, depending on the temperature range (associated with the presence or absence of drain leakage current), an increase or decrease of the responsivity is observed in subthreshold conditions. For the gate-injection (GI) configuration, as expected by the capacitive gate–drain coupling, the voltage responsivity at low frequency is null, but only for V_{GS} above threshold. Surprisingly, in subthreshold conditions, it is very high and positive, contrary to the negative values intuitively expected for this configuration. The origin of this unexpected behavior, taking place in both gate and drain injection (DI) configurations, is that the drain terminal is self-biased at the zero-current (ZC) operating point (V_{DS} being largely negative). An analytical model based on static coefficients obtained from dc measurements can explain the mechanisms behind the observed dependencies of the experiments.**

***Index Terms*— Device physics, GAN high-electron-mobility transistors (HEMTs), radio-frequency detection, responsivity model, subthreshold, zero-bias detector.**

I. Introduction

In THE last few years, high-electron-mobility transistors (HEMTs) based on AlGaN/GaN have been investigated for applications such as broadband communications [1], radar components [2], or space applications [3] because of their excellent frequency and power characteristics. In this work, AlGaN/GaN HEMTs are applied as microwave detectors in the mm-wave region over a wide range of temperatures [4], [5]. In [6] and [7], a complete review of the state-of-the-art of FET-based THz detectors and their applications is presented. We focus our attention on their properties as zero-bias detectors, where excess noise is avoided and no self-heating takes place.

Defects in GaN-based HEMT devices can produce temperature effects, such as negative threshold voltage shifts [8], device characteristics degradation in high temperatures [9], and inconsistent performance over a broad temperature range of operation. In particular, as we will show, when operating as microwave detectors, the behavior of the responsivity may significantly change with temperature depending on the ionization degree of acceptors in the buffer [10]. For a complete analysis, four different configurations must be considered, depending on whether current or voltage is detected (with short- or open-circuit drain terminals, respectively) and whether the RF power is injected into the drain or gate terminal, which we will denote as drain-injection (DI) and gate-injection (GI) configurations, respectively.

Voltage detection in the subthreshold region shows a complex behavior due to drain self-biasing, which can be very significant when the transistor has a proper pinch-off behavior [5]. Indeed, in the presence of drain leakage current through the buffer (as happens in GaN HEMTs at low T due to the nonionization of the acceptor ions of the buffer), the DI voltage responsivity in subthreshold conditions becomes almost null, instead of being high as expected for "good" transistors. However, while the subthreshold behavior within the DI configuration was well explained in [5], the GI case is not yet well understood. Some works have shown that the voltage response is suppressed in the subthreshold region due to loading or leakage current effects [11], [12], [13], but a general explanation of the detection mechanism in GI configuration is still lacking. In this contribution, using expressions for the responsivity based on the Taylor series expansion of the I_D–V_{DS} curves [14], [15], we can retrieve and explain the experimental results in all the different configurations where V_{DS} self-biasing plays a key role. While the Taylor series expansion can be used to represent both nonlinear current and charge sources of the devices [16], our approach is just based on static current coefficients.

II. Device Under Test and Experimental Setup

The sketch of the experimental setup is presented in Fig. 1, where a LakeShore CRX-VF cryogenic probe station is used to

Manuscript received 3 August 2023; revised 18 October 2023; accepted 9 November 2023. This work was supported in part by MCIN/AEI/10.13039/501100011033 under Grant PID2020-115842RB-I00. *(Corresponding author: Gaudencio Paz-Martínez.)*

Gaudencio Paz-Martínez, Ignacio Íñiguez-de-la-Torre, Héctor Sánchez-Martín, Sergio García-Sánchez, Tomás González, and Javier Mateos are with the Applied Physics Department and USAL-NANOLAB, Universidad de Salamanca, 37008 Salamanca, Spain (e-mail: gaupaz@usal.es; indy@usal.es; hectorsanchezmartin@usal.es; sergio_gs@usal.es; tomasg@usal.es; javierm@usal.es).

Philippe Artillan is with Université Grenoble Alpes, Université Savoie Mont Blanc, CNRS, Grenoble INP, IMEP-LAHC, 38000 Grenoble, France (e-mail: philippe.artillan@univ-smb.fr).

Color versions of one or more figures in this article are available at https://doi.org/10.1109/TMTT.2023.3333418.

Digital Object Identifier 10.1109/TMTT.2023.3333418

© 2024 The Authors. This work is licensed under a Creative Commons Attribution 4.0 License.
For more information, see https://creativecommons.org/licenses/by/4.0/

This article has been accepted for inclusion in a future issue of this journal. Content is final as presented, with the exception of pagination.

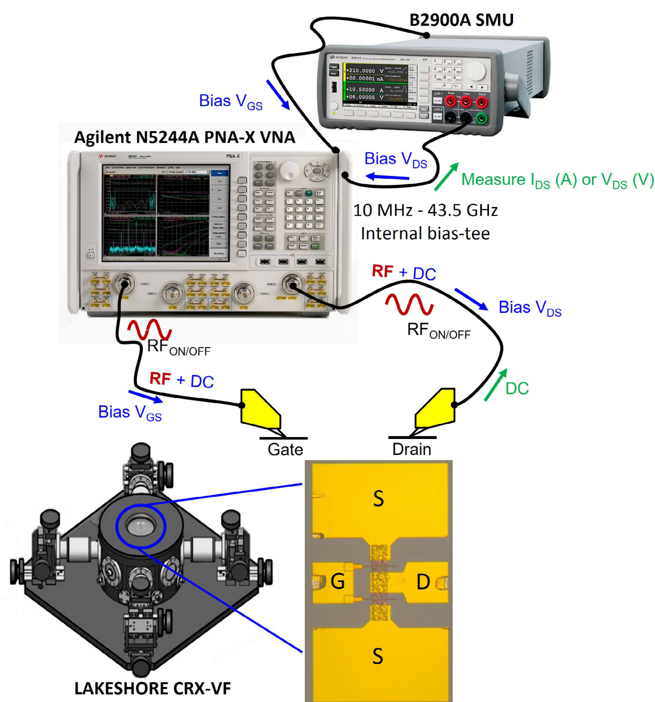

Fig. 1. Experimental setup. A cryogenic probe station is used to connect the VNA and the SMU to the device under test (the photography is presented in the sketch) through a GSG RF probe.

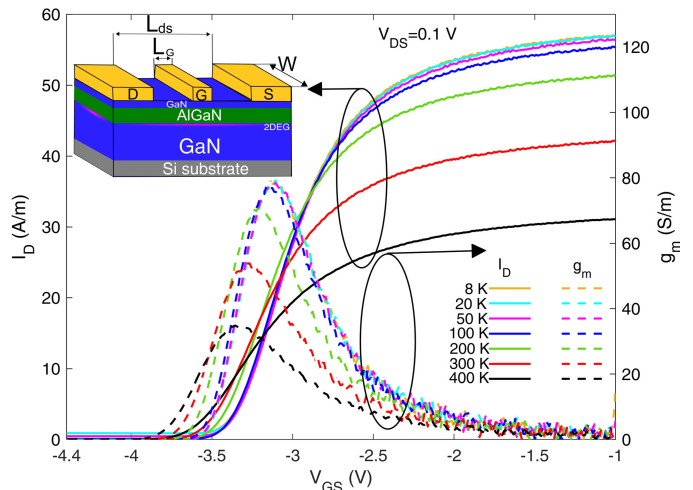

Fig. 2. I_D–$V_{\rm GS}$ (left axis) and corresponding transconductance g_m (right axis) of the HEMT under study for $V_{\rm DS} = 0.1$ V and temperatures from 8 to 400 K. A scheme of the transistor geometry is shown in the inset.

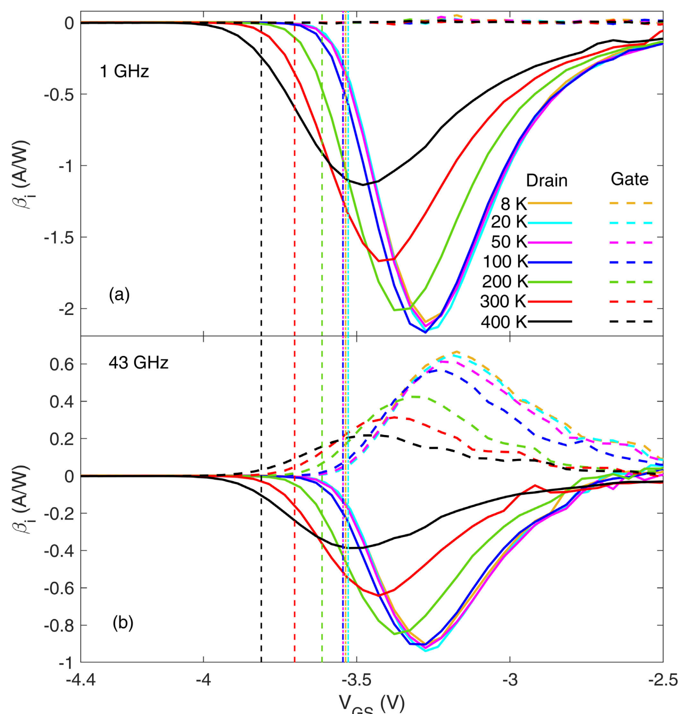

Fig. 3. ZV current responsivity (in A/W) measured at (a) 1 and (b) 43 GHz as a function of $V_{\rm GS}$ using both DI and GI configurations in the 8–400-K temperature range. The dashed vertical lines indicated the values of $V_{\rm th}$ for each temperature. The experiments were made with a small input RF power of −15 dBm injected to a GaN-HEMT with $L_G = 250$ nm and $W = 2 \times 25$ μm.

perform the measurements in a temperature range of 8–400 K. The layout contains coplanar-waveguide (CPW) accesses to contact the terminals with GSG RF probes. We focus our study on a AlGaN/GaN HEMT (inset in Fig. 2) grown on a high-resistivity silicon substrate whose details are provided in [5], [10], and [17]. A VNA Keysight N5244A has been used as an RF power source up to 43 GHz. The insertion losses of the cables and tips have been taken into account to actually deliver a constant RF power, P, at the reference plane of the transistor. The microwave signal in a 1–43-GHz span is injected either into the drain or the gate terminals. To bias both the gate and the drain of the transistor, a two-channel SMU B2902A is used. Two different modes for zero-bias detection will be used: zero-current (ZC) with an open-circuit drain, and zero-voltage (ZV) with a short-circuit drain. The responsivity in ZC conditions is obtained as the ratio $\beta_v = (\Delta V/P)$ and in ZV is $\beta_i = (\Delta I/P)$, where ΔV and ΔI are the dc shift caused by the RF excitation recorded always at the drain terminal and averaged during 5 s. Subscripts d or g are added to distinguish between DI and GI (β_{vd}, β_{vg}, β_{id}, and β_{ig}).

III. Results and Discussion

In Fig. 2, we show the I_D–$V_{\rm GS}$ curves and the corresponding transconductance (g_m) for a transistor with $L_G = 250$ nm and $W = 2 \times 25$ μm with $V_{\rm DS} = 0.1$ V over the temperature range of 8–400 K. The temperature has very little effect on the current, g_m, and threshold voltage ($V_{\rm th}$) at low T, up to 100 K [5]. Above, I_D and g_m decrease with increasing T, and also $V_{\rm th}$.

The ZV current responsivity in both DI and GI configurations versus $V_{\rm GS}$ always shows a bell shape with a maximum located 0.2–0.3 V above $V_{\rm th}$ and goes down to zero in subthreshold conditions regardless of T [Fig. 3(a) and (b)]. However, while β_{id} is flat at low frequency and then shows a high-frequency roll-off (results not shown here; see [17], [18]), β_{ig} is suppressed at low frequency due to the capacitive gate–drain coupling (the RF power needs to reach the drain to produce a nonzero response [18]). It is also remarkable that DI and GI configurations respond with opposite signs [see Fig. 3(b)].

This article has been accepted for inclusion in a future issue of this journal. Content is final as presented, with the exception of pagination.

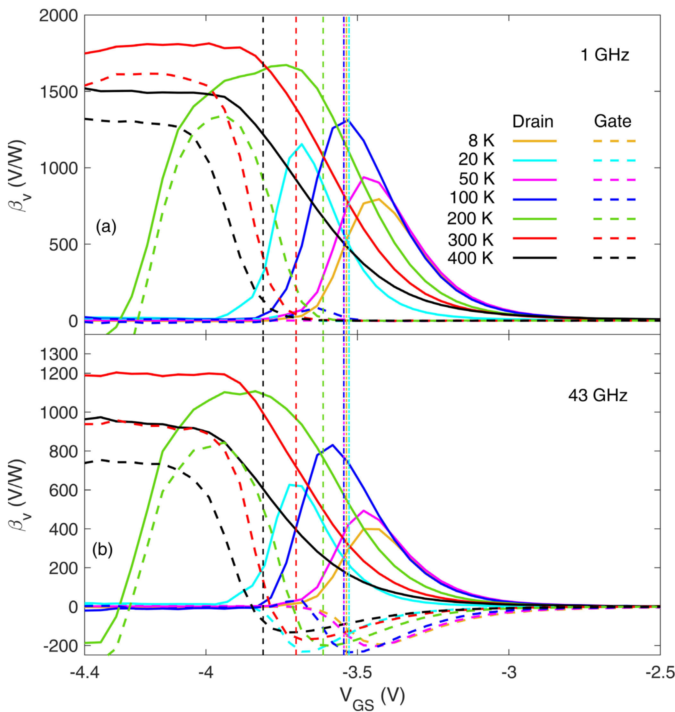

Fig. 4. ZC voltage responsivity (in V/W) measured at (a) 1 and (b) 43 GHz as a function of V_{GS} using both DI and GI configurations in the 8–400-K temperature range. The dashed vertical lines indicate the values of V_{th} for each temperature. The experiments were made with a small RF input power of -15 dBm injected to a GaN-HEMT with $L_G = 250$ nm and $W = 2 \times 25$ μm.

In the case of the ZC voltage responsivity [Fig. 4(a) and (b)], for $T < 200$ K, β_{vd} exhibits a bell shape with a positive maximum near V_{th}, being practically null in the subthreshold region, while for $T > 200$ K, it increases and saturates for $V_{\mathrm{GS}} < V_{\mathrm{th}}$. The origin of this behavior was already explained in [5]. It is due to the p-type doping of the GaN buffer, which is not active at low T, thus leading to an enhancement of the drain leakage current. In fact, a good transistor pinch-off leads to the self-biasing of the drain terminal due to the $I_D = 0$ bias condition, which is only fulfilled for negative V_{DS}, with the transistor entering into the third-quadrant-conduction region to generate a nonzero I_D able to compensate the always present (even if very small) gate leakage current. The most significant result of Fig. 4 is the behavior shown by β_{vg} in the subthreshold region for $T > 200$ K. Surprisingly, β_{vg} takes large positive values at 1 GHz, while a null value is expected due to the negligible gate–drain coupling at low frequency. In addition, the sign change of β_{vg} at high frequency was unexpected [see the transition of V_{GS} through V_{th} in Fig. 4(b)]. In [10], measurements of both responsivities over a wide temperature range are presented within the DI configuration for devices with different gate lengths.

To better understand the origin of these unexpected results, the frequency dependence of the ZC voltage responsivity at 300 K is plotted in Fig. 5(a) for DI and Fig. 6(a) for GI for two different bias points, one near pinch-off (but with the HEMT still conducting), $V_{\mathrm{GS}} = -3.61$ V $> V_{\mathrm{th}}$, and the other corresponding to subthreshold conditions, $V_{\mathrm{GS}} = -4.28$ V $< V_{\mathrm{th}}$. For DI [Fig. 5(a)], in both cases, β_{vd} shows a low-frequency plateau and then a high-frequency roll-off

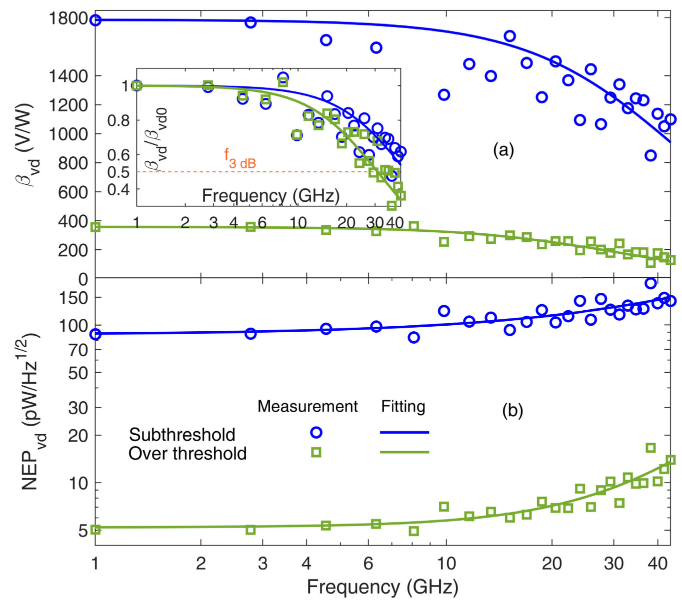

Fig. 5. (a) ZC responsivity at 300 K in DI for two values of V_{GS}: in subthreshold, $V_{\mathrm{GS}} = -4.28$ V $< V_{\mathrm{th}}$, and above threshold near pinch-off, $V_{\mathrm{GS}} = -3.61$ V $> V_{\mathrm{th}}$. The inset shows the normalized β_{vd} measurements (symbols) and data fittings (lines) to Lorentzians to extract the cutoff frequency. (b) NEP value for each case.

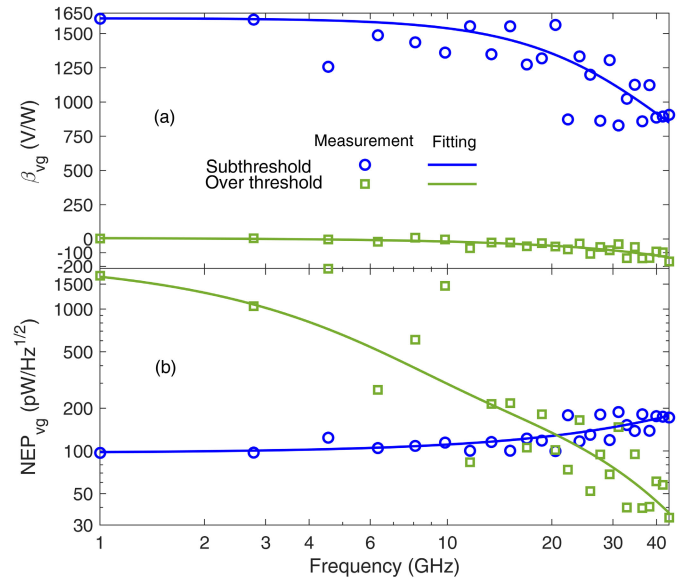

Fig. 6. (a) ZC responsivity at 300 K in GI for two values of V_{GS}: in subthreshold, $V_{\mathrm{GS}} = -4.28$ V $< V_{\mathrm{th}}$, and above threshold near pinch-off, $V_{\mathrm{GS}} = -3.61$ V $> V_{\mathrm{th}}$. (b) NEP value for each case.

which will be characterized by its 3-dB frequency, $f_{3\,\mathrm{dB}}$, for which a halved responsivity is obtained. The inset in Fig. 5(a) shows the $1/(1 + (f/f_{3\,\mathrm{dB}})^2)$ fitting. A value for $f_{3\,\mathrm{dB}}$ of 47 GHz is found in subthreshold conditions, much higher than that for $V_{\mathrm{GS}} > V_{\mathrm{th}}$, 31 GHz. On the other hand, in the case of GI [Fig. 6(a)], clear differences between the two operation regions are observed.

1) For V_{GS} above threshold, β_{vg} is null at low frequencies (up to $\approx$10 GHz), where it starts increasing. This high-pass filter behavior is expected for the GI configuration, since the gate–drain coupling is purely capacitive.

This article has been accepted for inclusion in a future issue of this journal. Content is final as presented, with the exception of pagination.

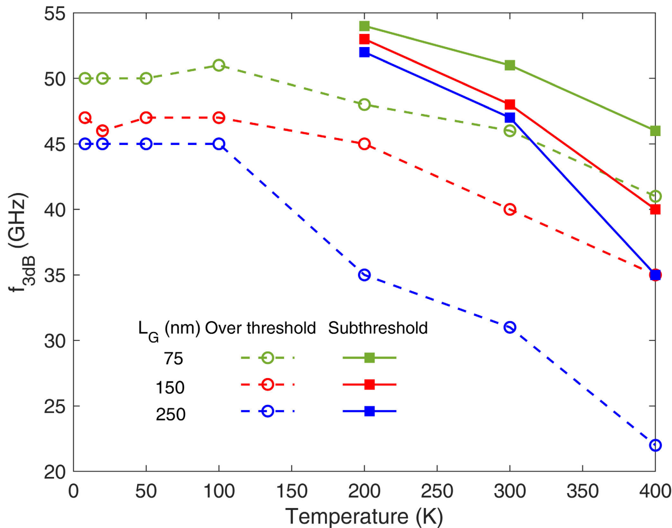

Fig. 7. Comparison of $f_{3\,\mathrm{dB}}$ for DI as a function of temperature for subthreshold (square symbol) and over threshold (circle symbol) gate bias conditions for three lengths of the gate, L_G.

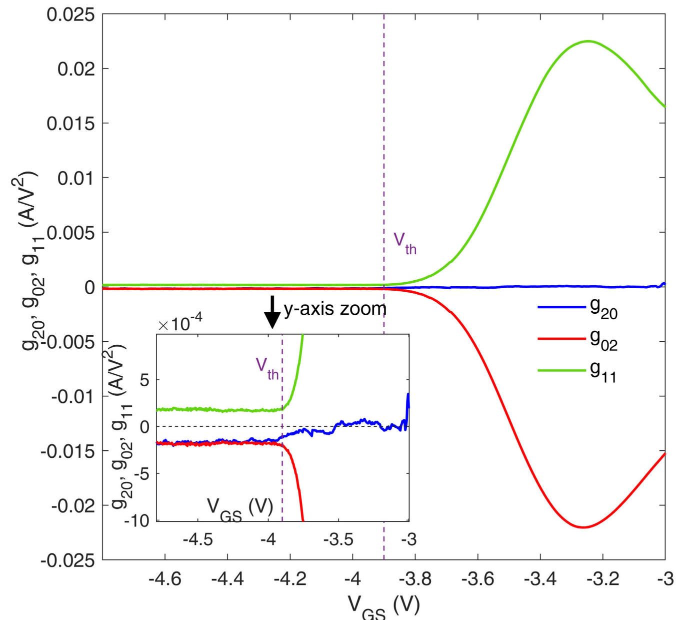

Fig. 8. Taylor series coefficients g_{02}, g_{20}, and g_{11} versus V_{GS} at 300 K. The vertical dotted line indicates the value of V_{th}. The inset corresponds to a zoom around the threshold.

2) In subthreshold conditions, the frequency dependence of β_{vg} resembles that obtained in DI, with a similar $f_{3\,\mathrm{dB}}$. Since such low-frequency response cannot be originated by the gate–drain coupling, the explanation for this result must be elsewhere.

In Fig. 5(b) for DI and Fig. 6(b) for GI, the noise equivalent power (NEP) corresponding to each responsivity curve is presented for both schemes (assuming equilibrium thermal noise, $\mathrm{NEP}_j = (4k_B T R_D)^{1/2}/\beta_{vj}$, with $j = d$, g, and R_D the resistance of the transistor). The lowest value of the NEP is found above the threshold as a consequence of the smaller resistance, 5 $\mathrm{pW/Hz^{1/2}}$ in DI ($f = 1$ GHz) and 33.9 $\mathrm{pW/Hz^{1/2}}$ ($f = 43$ GHz) in GI. This latter value would be even better at higher frequencies, above the frequency limit of our equipment, since the responsivity is still increasing and the NEP decreasing. For subthreshold conditions, this figure of merit takes similar values for both configurations of RF injection, with its best value around 90 $\mathrm{pW/Hz^{1/2}}$ obtained at low frequency and then increasing with the frequency roll-off of the responsivity.

The values of $f_{3\,\mathrm{dB}}$ for DI as a function of temperature are presented in Fig. 7 for three lengths of the gate, L_G. Note that $f_{3\,\mathrm{dB}}$ takes nearly constant values with V_{GS} both in the above threshold and in the subthreshold bias regions, with a distinct increase when entering the latter. However, this is only observed for $T > 200$ K since, for lower T, the responsivity is null in the subthreshold region. In this temperature range, $f_{3\,\mathrm{dB}}$ in both bias ranges increases when lowering T, saturating above the threshold at about 45 GHz for $\sim$100 K. We attribute such an increase of $f_{3\,\mathrm{dB}}$ to the enhancement of the mobility, which decreases the channel resistance.

In [18], we reported a generic high-frequency model of two-port RF detectors, based on static coefficients g_{ij} (defined as $g_{ij} = \partial^{(i+j)} I_D / \partial^i V_{\mathrm{GS}} \partial^j V_{\mathrm{DS}}$ and extracted from the measured I_D–V_{DS} curves) and measured S-parameters, able to replicate DI and GI responsivities by means of the following closed-form expressions:

$$\beta_{vd} = -\frac{R_0}{2g_{01}}\left(g_{20}|S_{12}|^2 + g_{02}|1+S_{22}|^2 + 2g_{11}\Re[S_{12}^*(1+S_{22})]\right) \quad (1)$$

$$\beta_{vg} = -\frac{R_0}{2g_{01}}\left(g_{20}|1+S_{11}|^2 + g_{02}|S_{21}|^2 + 2g_{11}\Re[S_{21}^*(1+S_{11})]\right) \quad (2)$$

where R_0 is the output impedance of the RF source.

Fig. 8 shows that for $V_{\mathrm{GS}} > V_{\mathrm{th}}$, g_{20} is null (due to the zero I_D bias conditions) and g_{02} and g_{11} have opposite signs and similar absolute values, with a maximum around $V_{\mathrm{GS}} = -3.23$ V. Remarkably, due to the capacitive gate–drain coupling, at low frequency $S_{12} = S_{21} = 0$, so that g_{02} is the only significant parameter for β_{vd} and g_{20} for β_{vg}. The fact that g_{20} is null allows the model to clearly explain the low-frequency behavior of both responsivities above the threshold, as well as the positive values obtained for β_{vd} and the negative ones for β_{vg}. At high frequency, $S_{12} = S_{21}$ (the transistor acts as a passive network since $V_{\mathrm{DS}} = 0$) increase, and consequently the (negative) contribution of the g_{11} terms, so that the roll-off of β_{vd} and the increase of β_{vg} (over threshold) observed in Figs. 5(a) and 6(a), respectively, are also well captured by the model.

However, below the threshold, one would expect to find that $\beta_{vg} = 0$ at low frequency [14], contrary to what it is obtained in the experiments [Fig. 4(a)]. The explanation is that g_{20} is not zero in those conditions (see the zoomed-in view of the inset of Fig. 8). In fact, it reaches a value close to that of g_{02} and with the same sign, so that β_{vd} and β_{vg} exhibit similar low-frequency behavior in the subthreshold region. The unexpected

This article has been accepted for inclusion in a future issue of this journal. Content is final as presented, with the exception of pagination.

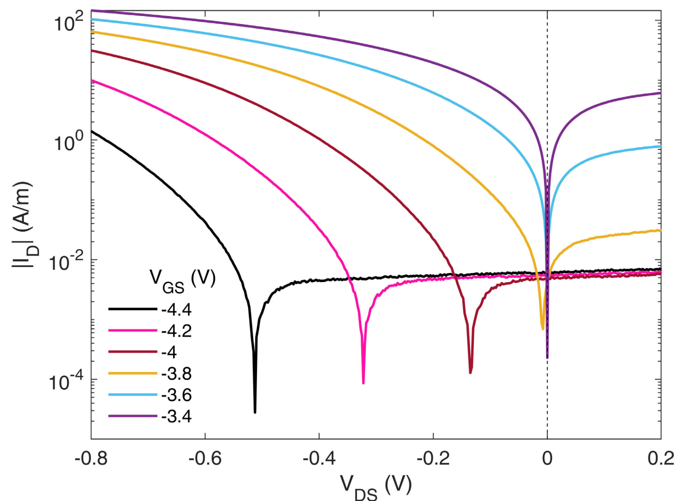

Fig. 9. Selected $|I_D|$–V_{DS} characteristic curves of the device for over threshold ($V_{\mathrm{GS}} = -3.4$ and -3.6 V) and subthreshold conditions ($V_{\mathrm{GS}} = -3.8$, -4, -4.2, and -4.4 V). The data corresponds to a GaN-HEMT with $L_G = 250$ nm and $W = 2 \times 25$ μm at 300 K.

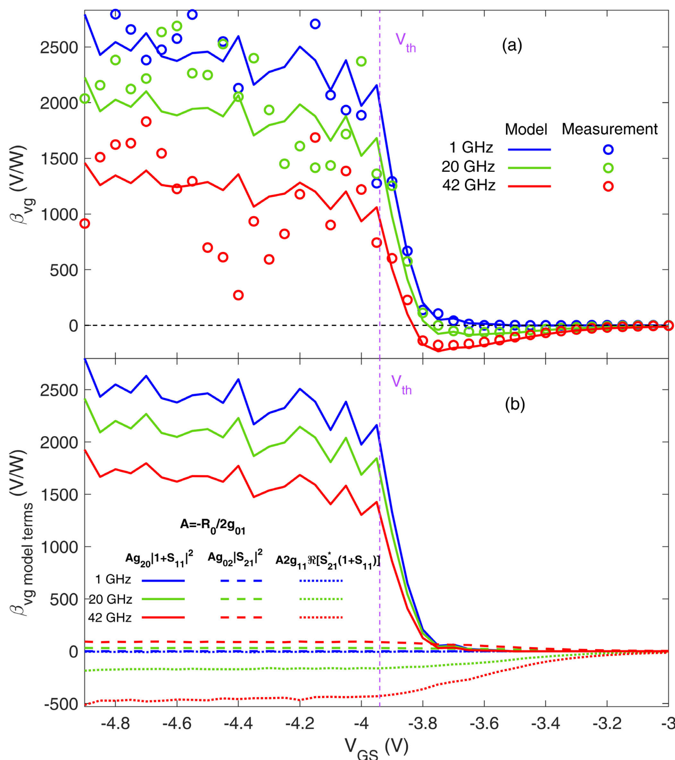

Fig. 10. (a) Comparison of the values of the ZC responsivity β_{vg} versus V_{GS} obtained in the experiments (symbols) with those calculated with (2) (solid line) at 300 K for 1, 20, and 42 GHz. The dashed vertical line indicates the value of V_{th}. (b) Representation of the three terms of (2) for 1, 20, and 42 GHz.

nonzero value of g_{20} occurs because for $V_{\mathrm{GS}} < V_{\mathrm{th}}$, the zero I_D point is shifted to negative values of V_{DS} (see Fig. 9, with the $|I_D|$–V_{DS} curves of the transistor in log scale). This behavior is related to the gate-leakage current and ionization of deep donor-like traps. This ionization starts around $T = 200$ K in C-doped GaN [5], the technology of the device under test. As a consequence, since the $I_D = 0$ point depends on V_{GS}, the value of $g_{20} = \partial^2 I_D / \partial^2 V_{\mathrm{GS}}$ is not null anymore for $V_{\mathrm{GS}} < V_{\mathrm{th}}$. The very good agreement found in the comparison of the

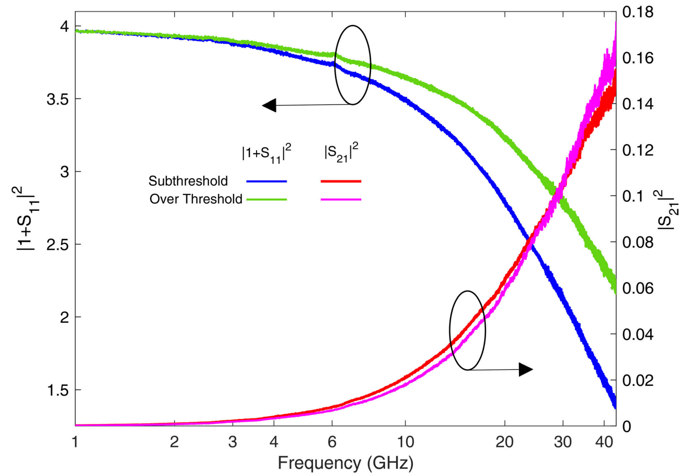

Fig. 11. $|1 + S_{11}|^2$ (left y-axis) and S_{21} (right y-axis) as a function of frequency for bias points in subthreshold ($V_{\mathrm{GS}} = -4.28$ V) and over threshold ($V_{\mathrm{GS}} = -3.61$ V).

experimental values of β_{vg} with those predicted using (2) for the whole V_{GS} range is shown in Fig. 10(a) at different frequencies. The corresponding terms of (2) are shown in Fig. 10(b). As expected, at 1 GHz (blue curves), only the term proportional to g_{20} contributes to the responsivity, since the second and third terms of (2) are null due to $S_{21} = 0$, as shown in Fig. 11, and therefore it is only significant in subthreshold conditions. When the frequency increases, S_{21} also increases and the second and third terms are no longer null, explaining the frequency roll-off observed in Fig. 6(a) (blue curve) but the first term is still the dominant one in subthreshold. With the increase in frequency, the first and the second terms add and counteract the effect of the third one. Finally, at $f = 42$ GHz (red curves), even though $|1 + S_{11}|^2$ is decreasing and the second and third terms increase, again the first term prevails. Therefore, below the threshold, the first term is always the dominant.

The roll-off of β_{vd} mentioned before, and observed in Fig. 4(a), is principally due to the fact that the coefficients g_{02} and g_{11} in (1) have opposite sign (see inset of Fig. 8). At high frequencies, the positive value of the third term increases and, when added to the negative value of the second term, it leads to a reduction of the (negative) responsivity. In subthreshold, the first term reinforces the second one, so that $f_{3\,\mathrm{dB}}$ increases.

IV. Conclusion

We have presented experimental results of zero-bias microwave power detection up to 43 GHz with GaN HEMTs both within the DI and GI configurations in a wide temperature range. While the dependencies of the detection on T, V_{GS} and frequency are well understood for $V_{\mathrm{GS}} > V_{\mathrm{th}}$, it is not the case in subthreshold conditions, where the drain self-bias plays a key role (mainly for $T > 200$ K). In fact, it allowed us to explain the subthreshold behavior of the responsivity β_{vg}. We remark that this mechanism also breaks the usual assumption that g_{20} is null in subthreshold, thus allowing us to explain several initially puzzling results, mainly the nonzero values of the responsivity β_{vg} at low frequency (where the gate–drain coupling is null). With all the terms of (2) correctly taken

This article has been accepted for inclusion in a future issue of this journal. Content is final as presented, with the exception of pagination.

into account, the dependence of the GI voltage responsivity on V_{GS} and frequency can be well reproduced by the model. From a practical point of view, our ZC results evidence that GI detection in the subthreshold region, in spite of increasing the responsivity at room temperature (and also increasing $f_{3\,\mathrm{dB}}$ within DI conditions), leads to NEP values much higher than over threshold, thus degrading the detector sensibility.

REFERENCES

[1] J. Moon et al., "55% PAE and high power Ka-band GaN HEMTs with linearized transconductance via n+ GaN source contact ledge," *IEEE Electron Device Lett.*, vol. 29, no. 8, pp. 834–837, Aug. 2008.

[2] K. Kikuchi et al., "An 8.5–10.0 GHz 310 W GaN HEMT for radar applications," in *IEEE MTT-S Int. Microw. Symp. Dig.*, Jun. 2014, pp. 1–4.

[3] P. Waltereit et al., "GaN HEMTs and MMICs for space applications," *Semicond. Sci. Technol.*, vol. 28, no. 7, Jun. 2013, Art. no. 074010.

[4] H. W. Hou, Z. Liu, J. H. Teng, T. Palacios, and S. J. Chua, "High temperature terahertz detectors realized by a GaN high electron mobility transistor," *Sci. Rep.*, vol. 7, no. 1, pp. 1–6, Apr. 2017.

[5] G. Paz-Martínez et al., "Temperature and gate-length dependence of subthreshold RF detection in GaN HEMTs," *Sensors*, vol. 22, no. 4, p. 1515, Feb. 2022.

[6] F. Aniel et al., "Terahertz electronic devices," in *Springer Handbook of Semiconductor Devices*. Berlin, Germany: Springer, 2022, pp. 807–849.

[7] E. Javadi, D. B. But, K. Ikamas, J. Zdanevicius, W. Knap, and A. Lisauskas, "Sensitivity of field-effect transistor-based terahertz detectors," *Sensors*, vol. 21, no. 9, p. 2909, Apr. 2021.

[8] M. S. Nazir, P. Kushwaha, A. Pampori, S. A. Ahsan, and Y. S. Chauhan, "Electrical characterization and modeling of GaN HEMTs at cryogenic temperatures," *IEEE Trans. Electron Devices*, vol. 69, no. 11, pp. 6016–6022, Nov. 2022.

[9] Y. Liang et al., "The interface trap analysis of AlGaN/GaN high electron mobility transistors with temperature based on conductance method," *J. Phys., Conf.*, vol. 2248, no. 1, Apr. 2022, Art. no. 012016.

[10] G. Paz-Martínez, I. Ìñiguez-de-la-Torre, H. Sánchez-Martín, T. González, and J. Mateos, "Analysis of GaN-based HEMTs operating as RF detectors over a wide temperature range," *IEEE Trans. Microw. Theory Techn.*, vol. 71, no. 7, pp. 3126–3135, Jul. 2023.

[11] W. Knap et al., "Nonresonant detection of terahertz radiation in field effect transistors," *J. Appl. Phys.*, vol. 91, no. 11, pp. 9346–9353, Jun. 2002.

[12] H. Kojima and T. Asano, "Impact of subthreshold slope on sensitivity of square law detector for high frequency radio wave detection," *Jpn. J. Appl. Phys.*, vol. 58, Mar. 2019, Art. no. SBBL05.

[13] M. Sakowicz et al., "Terahertz responsivity of field effect transistors versus their static channel conductivity and loading effects," *J. Appl. Phys.*, vol. 110, no. 5, Sep. 2011, Art. no. 054512.

[14] M. A. Andersson and J. Stake, "An accurate empirical model based on Volterra series for FET power detectors," *IEEE Trans. Microw. Theory Techn.*, vol. 64, no. 5, pp. 1431–1441, May 2016.

[15] M. I. W. Khan, S. Kim, D.-W. Park, H.-J. Kim, S.-K. Han, and S.-G. Lee, "Nonlinear analysis of nonresonant THz response of MOSFET and implementation of a high-responsivity cross-coupled THz detector," *IEEE Trans. Terahertz Sci. Technol.*, vol. 8, no. 1, pp. 108–120, Jan. 2018.

[16] S. M. Homayouni, D. M. P. Schreurs, G. Crupi, and B. K. Nauwelaers, "Technology-independent non-quasi-static table-based nonlinear model generation," *IEEE Trans. Microw. Theory Techn.*, vol. 57, no. 12, pp. 2845–2852, Dec. 2009.

[17] G. Paz-Martínez et al., "Comparison of GaN and InGaAs high electron mobility transistors as zero-bias microwave detectors," *J. Appl. Phys.*, vol. 132, no. 13, Oct. 2022, Art. no. 134501.

[18] G. Paz-Martínez, P. Artillan, J. Mateos, E. Rochefeuille, T. González, and I. Ìñiguez-de-la-Torre, "A closed-form expression for the frequency dependent microwave responsivity of transistors based on the I–V curve and S-parameters," *IEEE Trans. Microw. Theory Techn.*, early access, Jul. 14, 2023, doi: 10.1109/TMTT.2023.3291391.